Mesoscopic sponge-like topology engineered onto polypropylene promotes retention of bound protein: Material synthesis, characterization and utility

Alpay Taralp,[*1] *Döne Demirgöz,*[2] *Wolfgang Voelter*[2]

[1]Materials Science and Engineering Program, Faculty of Engineering and Natural Sciences, Sabancı University, Istanbul, 34956 Turkey; Fax: (+90) 216 483 9550; E-mail: taralp@sabanciuniv.edu
[2]Interfakultäres Institut für Biochemie, Eberhard-Karls-Universität Tübingen, Hoppe-Seyler-Straße 4, Tübingen D-72076, Germany

Summary: A simple synthetic approach was developed to transform ordinary polypropylene tubes into high-surface, protein-retaining plastics. The inner surface of native tubes was activated by incubation with aqueous persulfate. Infrared spectroscopic analyses of plastics treated in this fashion revealed significant amounts of carboxylic acids, ketones and alcohol groups as products. Concomitant to activation, a transformed surface was yielded, which displayed a meso-structured, high-area topology. The topology, reminiscent to the appearance of natural sponge, appeared to have been caused by an oxidation-induced phase separation. The enhanced chemical reactivity of oxidized surface-pendent functional groups greatly facilitated re-engineering of surface physico-chemical traits. The oxidized surfaces were treated with the hydrolysis products of aminopropyltriethoxysilane, and ninhydrin or glutaraldehyde, affording the corresponding amino and aldehyde surface derivatives. The performance of each tailored surface was assessed by the extent to which albumin could be loaded and retained following several washings. The results of the immobilization study indicated that appropriately engineered mesoscale topologies could greatly improve the retention of non-covalently adhered proteins. A model is proposed to rationalize the contribution of the mesostructure to protein binding.

Keywords: albumin; biocompatibility; mesoscopic; oxidation; persulfate; phase separation; protein adsorption; smart plastics

Introduction

The interaction between biomolecules and plastic surfaces defines an area of much interest. In keeping with this theme, established methods continue to be used to fine-tune the surface traits of low surface energy plastics such as polypropylene [1]. Nonetheless, more approaches are required to facilitate the engineering of mesoscale or nanoscale-sized surface structures along plastics.

In this study, the oxidative activation, surface engineering and protein-retaining ability of

modified polypropylene tubes was examined. The plastics were first transformed using reagents of established reactivity, yielding surfaces with different physico-chemical traits (figure 1). Subsequently, the plastics were wetted with protein solutions under conditions that would permit protein-surface interaction. The novelty of this work was related to the fact that one of the chemical steps, specifically oxidation, afforded surfaces, which were markedly different in topology and better able to retain adsorbed protein in comparison to conventionally used flat surfaces. Bovine serum albumin was used as test protein in view of the potential of surface-bound human serum albumin to biocompatibilize man-made materials.

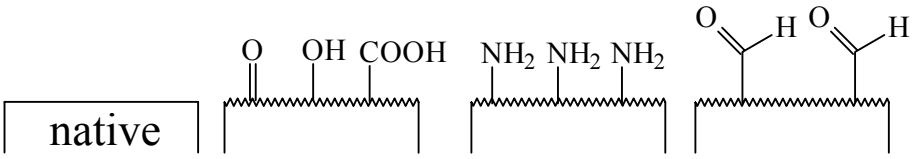

Figure 1. Summary of proposed chemical reactions to yield new surfaces. Beginning with native isotactic polypropylene (A), oxidation affords surface carboxyl, alcohol and keto groups (B), aminopropylsilylation affords aminopropyl groups (C) and ninhydrin-induced deamination yields propanal groups (D). The texture of native surface A has been depicted as smooth in contrast to all subsquent surfaces, which have been drawn rippled in comparison, to denote the unexpected and marked changes of topology during oxidation.

Experimental

Materials. Eppendorf Safe-Lock brand plastic tubes (2ml capacity) were obtained from Eppendorf GmbH. Dialysis bags (3500 molecular weight cut-off) were obtained from Pharmacia. Bovine serum albumin, distilled water, solvents and reagents were obtained from Sigma-Aldrich Chemie GmbH.

Oxidative activation of Eppendorf tubes and characterization of derivatives. Tubes comprised of injection-molded isotactic polypropylene were used. Aqueous persulfate solution was delivered so that each tube was filled to half capacity. The tubes were closed tightly, incubated without motion (70ºC, 0-24h), and flushed thoroughly with water. The inner surfaces were rinsed once with isopropanol and dried in a vacuum. Control surfaces were treated similarly except that inert ammonium sulfate was used in place of persulfate.

Aminopropylsilylation of activated Eppendorf tubes. Tubes were incubated (20min) in solution of the composition aminopropyltriethoxysilane/water/isopropanol (1:4:95) during which time reactive silanol species formed *in situ*. The tubes were decanted, refilled fully with isopropanol, decanted, refilled and decanted. Silanol retained on the surface was

cured overnight, affording aminopropylsilyl surfaces. The tubes were flushed in water and dried. Control surfaces were treated similarly. Surface amination was quantified (575nm) against known amounts of aminopropyltriethoxysilane in a 1% propanolic solution of ninhydrin (70°C, 1h).

Aminopropylsilylated surfaces transformed to the aldehyde via reaction with ninhydrin or glutaraldehyde. Accessible aminopropylsilyl moieties were de-aminated and transformed into propanal moieties by reaction with a freshly prepared 1% ninhydrin solution in n-propanol. All surfaces were flushed with water and ethanol, and dried. Native/ammonium sulfate control surfaces were also treated with ninhydrin. In the case of glutaraldehyde, an aqueous 2% stock was pre-activated at pH 10 and reset 4h later to pH 8. The solution was applied directly to aminopropylsilylated surfaces (25°C, 1h). The tubes were flushed with water and ethanol, and allowed to dry.

Protein binding studies. Heat-shock fractionated albumin (100mg) was dissolved in water (10ml) and the pH value of solution was raised to 9 using sodium hydroxide (1M). A 5% (w/v) solution of dansyl chloride (5-dimethylamino-1-naphthalenesulfonyl chloride) in acetonitrile (100μl) was delivered to the stirred solution. After 1h, the solution was delivered into a dialysis bag and dialyzed once against 4L of buffer (25°C, 50mM sodium phosphate, pH 7) and twice against 4L distilled water. Ninhydrin color analysis of native albumin and derivatized albumin (50μl dialyzed solution in 950μl of 1% ethanolic ninhydrin, 70°C, 1h) indicated that at most 10% of the amino groups had been transformed into the sulfonamide fluorophore. The dansylated protein stock was stored at 4°C. An aliquot of trace-dansylated bovine albumin (0.3mg protein/ml, pH 8.5) was delivered to the tubes, which were inverted manually on occasion (25°C, 2h) before being emptied. The tubes were washed in salt solution under manual inversion and decanted. A second high salt wash was performed. The tubes were agitated subsequently with water and decanted. Lastly, the tubes were incubated with 10% Triton X100 and water. The tubes were photographed under UV light following each step of the workup.

Scanning electron microscopy of functionalized Eppendorf tubes. Processed samples were cleaned thoroughly and coated (25s) with gold using an Agar brand sputterer, affording a coating of an approximate 20nm thickness. Scanning electron micrographs were obtained using a JEOL model JSM-6500F instrument with a beam voltage of 10-20kV. At least four areas per sample were examined at resolutions up to 50000X and analyzed using windows-based imaging software. Native tubes were coated using silver as opposed to

gold but either metal greatly enhanced the image contrast between surface and air.

Surface characterization using ATR-FTIR spectroscopy. Samples were dried in a vacuum oven prior to analysis to purge moisture and other volatiles from the matrix of the plastic. Clear regions of samples were tightly clamped over the window of the attenuated total reflectance (ATR) accessory of a Bruker model Equinox 55 infrared spectrophotometer. Twenty scans were averaged using a 70-point rubber-band correction option. To assess the oxidation state of underlying layers, sample surfaces were subjected to abrasion. Prior to each analysis, the thickness removed was quantified using a micrometer.

Fluorescence imaging of immobilized dansyl-albumins. Eppendorf tubes were placed upon a broadband light table centered at 312nm and photographed using black & white Polaroid film. The camera was mounted on a model DSH7 square pyramid multiplier hood with a rating of 0.7X. Images were shot with a Polaroid GelCam fitted with a Tiffen #15 deep yellow filter.

Results

Figure 2 illustrates the attenuated total reflectance spectral profiles of native and 16h-oxidized polypropylene. The post-oxidation profile (Fig. 2, solid line) showed changes in the functional group region (4000-1300cm^{-1}), fingerprint region (1300-900cm^{-1}), and remaining low-frequency region (900-600cm^{-1}). Three distinct carbonyl types were noted. On the basis of spectral data and established reaction chemistries, the oxidation products appeared to be limited to alcohol, ketone, carboxylic acid and potentially ester groups [?]. Time-course oxidation profiles (not shown) yielded a monotonic increase of signal, with maximal intensities being reached after 18h of reaction. As reaction times increased, signs of oxidation were noted at greater penetration depths. By 16h of reaction, oxidation products were noted downwards of 100 microns, far exceeding the typical depth of the skin layer and entering the realm of core material. Stretching frequencies consistent with the oxidation products of polypropylene included those of alcohol ($\nu_{O\text{-}H\ isolated}$ = 3640-3610cm^{-1} ; $\nu_{O\text{-}H\ H\text{-}bonded}$ = 3420-3250cm^{-1}; $\nu_{C\text{-}O\text{-}H\ bending}$ = 1440-1260cm^{-1}; $\nu_{C\text{-}O}$ = 1160-1030cm^{-1}), ketone ($\nu_{C=O}$ = 1725-1705cm^{-1}), carboxylic acid ($\nu_{O\text{-}H\ isolated}$ = 3550-3500cm^{-1}; $\nu_{O\text{-}H\ H\text{-}bonded}$ = 3300-2500cm^{-1}; $\nu_{C=Omonomer}$ = 1780-1740cm^{-1}; $\nu_{C=Odimer}$ = 1710-1690cm^{-1}; $\nu_{stretchC\text{-}O}$ = 1320-1210cm^{-1}; $\nu_{bendC\text{-}OH}$ = 1440-1400cm^{-1}), ether ($\nu_{C\text{-}O}$ = 1140-1110cm^{-1}) and ester functional groups ($\nu_{C=O}$ = 1765-1720cm^{-1}; $\nu_{C\text{-}Oacid}$ = 1280-

1150cm^{-1}; $\nu_{C\text{-}Oalcohol}$ = 1150-1000cm^{-1}) [?]. Detectable levels of aldehyde functional groups had not accumulated in view that the Fermi doublet was not observable. Along the surface of the plastic, transformed functional groups included ketone, carboxylic acid and alcohol groups (see discussion for further explanation).

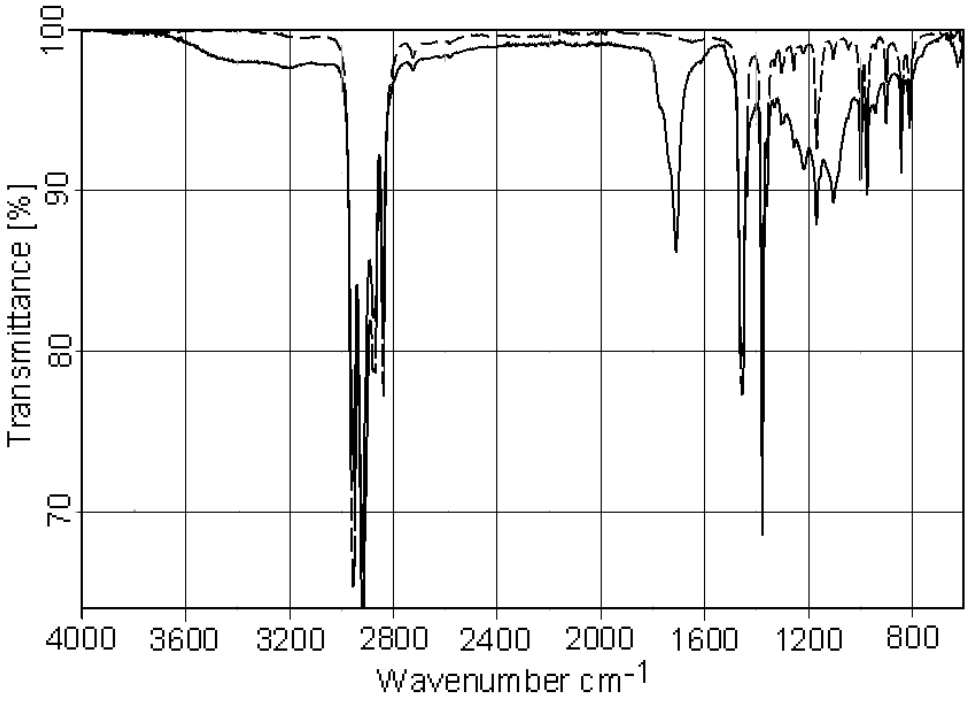

Fig. 2. ATR FT-IR spectrum of vacuum-dried polypropylene samples before (dashed line) and after (solid line) treatment with persulfate solution (1M, 70°C, 16h).

Oxidized surfaces, treated with the hydrolysis products of aminopropyltriethoxysilane, tested positive with ninhydrin. Similarly treated native tubes and ammonium sulfate blanks tested ninhydrin negative, showing by contrast, that oxidation had led to bonding of the organosilane reagent. Quantitative ninhydrin analysis of each tube indicated an approximate loading of 200nmole of amino groups/frontal cm^2. In this respect, amine loadings were significantly higher than those measured along commercially produced flat surfaces. To assess the thermal and solvent stability of the new layer, aminopropylsilylated tubes were incubated in water, dimethylformamide, or *p*-xylene (1.8ml, 2h, 70ºC). The liquid phase tested negative with ninhydrin, indicating that amino groups were fully retained on the surfaces during the incubation period. Samples tested up to 6 months following aminopropylsilylation afforded comparable color yields, suggesting that the new layer was also stable in time.

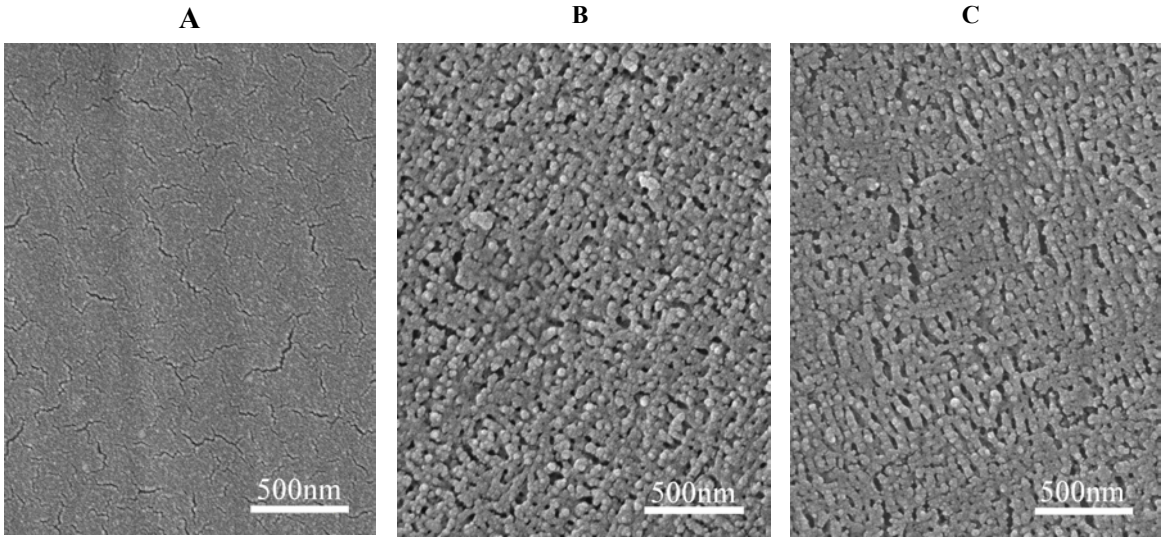

Figure 3. Scanning electron micrographs of gold-coated surfaces of Eppendorf tubes treated 16h with ammonium sulfate (A), persulfate (B) and persulfate followed by the hydrolysis products of aminopropyltriethoxysilane (C).

Figure 3 contrasts the appearance of native (A), 16h-oxidized (B), and subsequently aminopropylsilylated polypropylene (C). The native surface appeared smooth at the mesoscopic length-scale, with exception to some minor cracking, which were artifacts of the silver coating. In contrast, the 16h-oxidized surface illustrates a natural sponge-like appearance. Micrograph images at shorter oxidation times (not shown) showed native-like surfaces over the first 8h of oxidation, whereas minor changes of topology had developed by 10h, in the form of sparsely distributed mesoscale bulges. A brief period of dramatic change occurred thereafter, as evidenced by a sponge-like mesoscale topology at 12h. The sponge-like appearance did not change thereafter up to the final 24h time point. The topology of 16h-oxidized and aminopropylsilylated material (Fig. 3C) appeared slightly denser than the oxidized starting material (Fig. 3B). Assuming that a gold coating of comparable thickness was overlaid in the sputterer, the difference would be consistent with the overlay of a thin aminopropylsiloxane-silanol layer.

Once the aminopropylsilyl groups were incubated with ninhydrin or particularly glutaraldehyde, spectroscopic measurements could no longer detect a subtle N-H scissoring frequency at 1550cm^{-1}. Also, a carbonyl stretching signal about 1720-1700cm^{-1} had increased, consistent with the accumulation of aldehydes. Color was not yielded during a second incubation with fresh ninhydrin, implying that accessible primary amino groups within the aminopropylsiloxane-silanol matrix had indeed reacted with ninhydrin or glutaraldehyde.

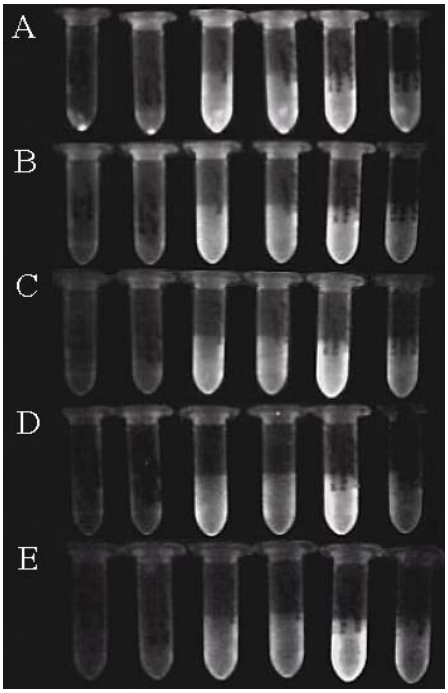

Figure 4. Binding of trace-dansylated albumin. Columns from left to right: Native polypropylene; ammonium sulfate-treated polypropylene; oxidized polypropylene; oxidized and aminopropylsilylated polypropylene; ninhydrin treated aminopropylsilylated polypropylene; and, glutaraldehyde-treated aminopropylsilylated surfaces. Rows (A-E) distinguish the different steps of the wash procedure: Protein solution (1ml) was incubated (20min) and decanted (A); Tubes were agitated with 1M NaCl (1ml, 5min) and the solution was decanted (B); a second NaCl washing was performed (C); tubes were agitated with water (1ml, 5min) and the solution was decanted (D); tubes were agitated with 10% triton X100 (1ml, 5min) and the solution was decanted (E).

Protein binding studies were performed on native and tailored tubes as indicated in figure 4. The performance of three sponge-patterned derivatives in particular could be assessed by the extent to which trace-labeled fluorescent albumin remained surface-bound following adsorption and repeated washings. The oxidized, aminated and aldehyde-bearing surfaces yielded strong fluorescence, even after several washings. On the basis of fluorescence intensities, propanal-mediated loadings appeared to be greater than glutaraldehyde-mediated immobilization. Decanted wash solutions displayed no noticeable fluorescence, which might have indicated significant leaching. Oxidized polypropylenes, which had not yet phase-separated, were similarly engineered with surface amino and aldehyde groups to confirm or rule out any advantage of a sponge-like topology in the matter of retaining protein. Flat aminopropylsilylated surfaces lost all fluorescence after the washings, albeit not as quickly as did native control surfaces. Commercially available plasma-aminated flat surfaces performed similarly. In contrast,

oxidized and aldehyde-pendant flat surfaces still retained strong fluorescence, presumably by forming imine bonds with protein. Apparently, a sponge-like topology bearing amino groups permitted protein retention in the absence of covalent bonding.

Discussion

Persulfate-initiated oxidative activation of polypropylene. In attempting to rationalize the infrared profiles depicted in figure 2, polypropylene oxidation in general was necessarily re-examined. Free radical oxidation or air-induced auto-oxidation of polypropylene is complex and much work has been devoted to examining thermally-induced or photo-chemical changes, particularly in the absence of water. The experimental conditions used herein differed markedly from those typically employed to simulate polyolefin degradation. The time-scale of changes was much shorter, the concentration and oxidation potential of the oxidant was relatively high, the reaction environment at the surface and immediate sub-surface differed notably from that of deeper regions, and the activation of hydroperoxide by ultraviolet light was avoided, as well as were any Norish type I and II mechanisms. Despite these differences, polypropylene oxidation generally yields a handful of similar functional group products, irrespective of the mode of oxidation. For instance, alcohol, carboxylic acid and ketone functional groups are noted during long-term degradation under atmospheric conditions. These have also been noted under markedly different conditions, where polypropylene has been deliberately oxidized by aqueous solutions of chromate or peroxyacids, or by reactive plasmas. In light of the consistency of these findings, oxidation products such as alcohol, ketone and carboxylic acid groups were similarly anticipated following treatment with persulfate and their detection was therefore not surprising. Aldehyde groups were not anticipated under the conditions employed, due to their high reactivity with neighboring groups and propensity to yield esters subsequent to their formation. A significant accumulation of vinyl and vinylidene groups was discounted in view that olefinic signatures in the infrared spectrum were either too weak to be detected, or alternatively, masked by stronger signals. Moreover, such transformations are typically promoted under anoxic conditions [?]. Accumulation of hydroperoxide groups, particularly at the surface, was neither observed nor anticipated, due to the contribution of competing decomposition reactions.

$^{-}O_3SO\text{-}OSO_3^{-} \rightarrow 2SO_4^{\cdot -}$	(1)	classic aqueous-phase initiation
$SO_4^{\cdot -} + H_2O \rightarrow HSO_4^{-} + \cdot OH$	(2)	propagation in aqueous-phase
$RH + SO_4^{\cdot -} \rightarrow R\cdot + HSO_4^{-}$	(3)	propagation at surface via H-abstraction
$RH + SO_4^{\cdot -} \rightarrow RH^{\cdot +} + SO_4^{2-} \rightarrow R\cdot + H^+ + SO_4^{2-}$	(4)	propagation at surface via e^- abstraction
$RH + \cdot OH \rightarrow R\cdot + H_2O$	(5)	propagation at surface via H-abstraction
$R\cdot + O_2 \rightarrow R\text{-}OO\cdot (+ HR') \rightarrow R\text{-}OOH + \cdot R'$	(6)	propagation in polymer via back-biting
$R\text{-}O\cdot \rightarrow$ **R'=O** $+ \cdot R''$	(7)	propagation in polymer via scission
$R{=}O + \cdot OH \rightarrow$ **R'(=O)OH** $+ \cdot R''$	(8)	propagation in/along polymer via transfer
$R{=}O + \cdot OR' \rightarrow$ **R"(=O)OR'** $+ \cdot R'''$	(9)	propagation through polymer via transfer
$RH + \cdot O\text{-}R' \rightarrow R\cdot +$ **HO-R'**	(10)	propagation through polymer via transfer
$HR\text{-}OOH + \cdot OOR' \rightarrow$ **R=O** $+ \cdot OH + HOO\text{-}R'$	(11)	propagation via radical-mediated decomposition
$HR\text{-}OOH + \cdot OH \rightarrow$ **R=O** $+ \cdot OH + H_2O$	(12)	propagation via radical-mediated decomposition
$R\text{-}OOH \rightarrow R\text{-}O\cdot + \cdot OH$	(13)	thermal decomposition in polymer
$R\text{-}OOH + HOO\text{-}R' \rightarrow R\text{-}O\cdot + \cdot OO\text{-}R' + H_2O$	(14)	thermal decomposition in polymer
$R\text{-}OOH + H^+ \rightarrow$ **R'=O** $+$ **HO-R"** $+ H^+$	(15)	acid-catalyzed decomposition in polymer
$HR\text{-}OOH + H^+ \rightarrow$ **R=O** $+ H_2O + H^+$	(16)	acid-catalyzed decomposition in polymer
$R\cdot + \cdot O\text{-}R' \rightarrow$ **R-O-R'**	(17)	termination
$R\cdot + \cdot OH \rightarrow$ **R-OH**	(18)	termination
$R\text{-}OO\cdot + \cdot OO\text{-}R'H \rightarrow$ **R-OH** $+$ **O=R'** $+ O_2$	(19)	termination
$RO\cdot + \beta\text{-}HR'OO\cdot \rightarrow$ **R-OH** $+$ **O=R"** $+ O{=}R'''$	(20)	termination
$HR\text{-}O\cdot + \cdot OH \rightarrow$ **R=O** $+ H_2O$	(21)	termination
$2\ HO\cdot \rightarrow \frac{1}{2}\ O_2 + H_2O$	(22)	termination

Figure 5. Solution-phase originating oxidation model illustrating alcohol, ketone, carboxylic acid, ester and ether formation in polypropylene (products in bold).

Figure 5 illustrates some established reactions, which could potentially contribute to yield the proposed products. Carbon centers (e.g., HR, R·) are generally depicted as tertiary but they may also be secondary, particularly with radical backbiting mechanisms (reaction 6), and primary on occasion. The HR-OOH group specifically depicts a secondary carbon center. An abstractable hydrogen beta to an active center, $\beta\text{-}H_{R'OO\cdot}$, is depicted (reaction 20). While others depict two initial modes of carbon radical formation (reactions 3-5), hydroxyl attack (reaction 5) is presumed to dominate. Processes leading to bond breakage and eventual phase-separation are outlined with italics. Since polyolefin oxidation is mediated by hydroperoxide decomposition, a special interest rests on characterizing the fate of hydroperoxide intermediates. The persulfate-polypropylene reaction describes a particularly interesting system, as hydroperoxide intermediates are likely decomposed to different extents as a function of spatial position. Deep within the polymer matrix, thermal homolytic cleavage and possibly heterolytic acid-catalyzed decomposition modes apply, whereas hydroperoxides positioned nearer to the surface are likely to face an increased concentration of carboxylic acid and mineral acid. Elucidating the pathways, which underlie various oxidation profiles, will form the basis of a subsequent manuscript

wherein a detailed attempt will be made to integrate the potential contributions of established chemical transformations (figure 5) and possibly their spatial dependency.

Functional groups pendent to the surface of oxidized polypropylene. Attenuated total reflectance infrared spectroscopic analysis quantifies functional groups within the skin layer of the polypropylene as opposed to quantifying the surface groups. As with most other bulk measurement techniques, surface functional groups cannot be examined directly using this method. That being said, carboxylic acid, ketone and hydroxyl functional groups were nonetheless anticipated at the surface of oxidized polypropylene. Attempts were not made to detect these surface groups directly, as the indirect evidence provided by attenuated total reflectance infrared spectroscopy and enhanced chemical reactivity was deemed sufficient. When considering the aqueous chemistry of persulfate, oxidative transformations necessarily begin at the surface and descend into the underlying layers of the material, assisted in particular by an established radical back-biting mechanism (figure 5, reaction 6). Moreover, when considering the conditions employed, the surface clearly remains a region that endured continuous oxidation. Thus, it follows to reason that the yield of surface-pendent functional groups should at least retain the essential elements of transformations noted in the bulk material, albeit, the relative ratio of surface and bulk oxidation products are probably subject to variation. Unlike acid, ketone and hydroxyl groups, surface ester groups were not anticipated in light of the hydrolytic and hydroxyl radical-rich aqueous environment, which would preclude any accumulation.

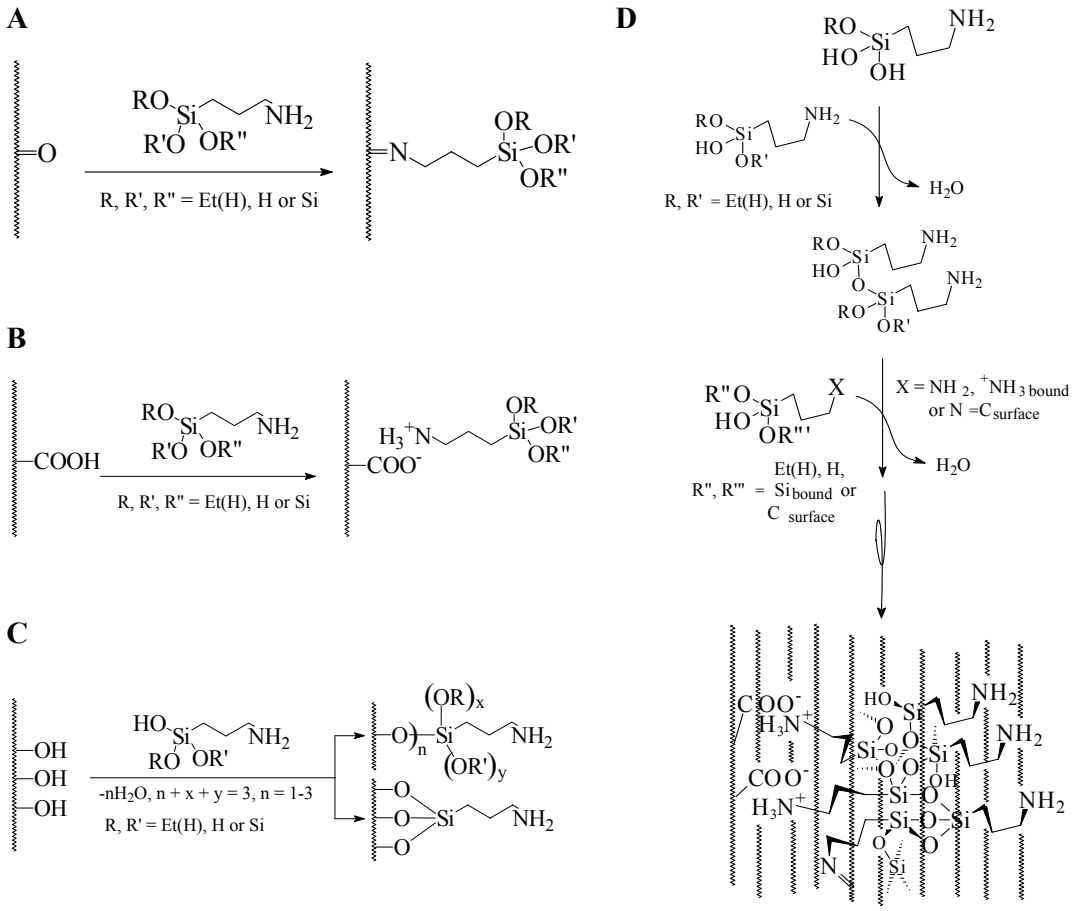

Figure 6. Four modes potentially contributing to the aminopropylsilylation of oxidized polypropylene. (A) Interfacial imine formation between surface carbonyl groups and amino groups of aminopropylsilyl species, (B) interfacial ammonium carboxylate ionic bonding between the conjugate base of surface carboxylic acids and protonated ammonium moieties of various aminopropylsilyl species, (C) interfacial condensation between surface hydroxyl groups and silanol groups of various aminopropylsilyl species, and (D) shape-conforming siloxane bonding of aminopropylsilyl species along the surface of polypropylene.

Aminopropylsilyation of activated surfaces. In view that the activated plastic potentially bore surface carboxylic acid, ketone, and hydroxyl groups, a reagent was sought that could interact and bind to each of the three functional group types. Aminopropyltriethoxysilane was ideal, as its hydrolytically activated form could potentially interact with ketone, carboxylic acid and hydroxyl groups, forming imine, ionic, and C-O-Si bonds, respectively. The choice was also suitable from the viewpoint of established organosilane coupling reactions in that a 3-8 monolayer hydrogen-bonded film of aminopropylsilyl species would typically be deposited along substrate materials under the experimental conditions employed. In solution and during curing phase, these surface-bound aminopropylsilyl species and overlaying aminopropylsilanol groups have a very high

propensity to self-condense as a Si-O-Si aminopropylsiloxane-silanol hydrate network. Moreover, the hydrogen-bonded network would be anticipated to conform to precise surface features in the process of curing, thus enforcing a fourth possible mode of bonding through shape complementarity. It followed to reason that once cured, a topmost surface layer, rich in amino groups and void of carboxylic acids or ketones, would be realized. The description of four possible binding modes is illustrated in figure 6. Indeed, the unusually high ninhydrin color yield of the cured surface supported the notion that amino groups were numerous along the sponge-like topology and readily solvent accessible. The positive outcome of the aminopropylsilylation step merited additional emphasis, as it showed clearly that roughened surfaces may be chemically engineered conveniently and effectively as are smooth surfaces. Normally, rough surfaces are not wetted as easily as smooth surfaces. In fact, in extreme cases a potential well literally pins a solvent front and retards its further advancement into a crevice. The findings supported the notion that the mesoscale crevices bore at least some hydrophilic character.

Origin of the mesopattern. Figure 3 highlighted a remarkable surface transformation, which was too sudden to have arisen from polymer degradation alone. A more likely cause was the abrupt release of material stress, which had accumulated during oxidation. Given the brevity of transformation and final appearance, the stress had clearly triggered a phase separation. Given the delay prior to phase separation, the stress must have arisen from the incremental buildup of oxidation products and voids in the matrix. Such signs of degradation are well characterized in polyolefins. Other signs of released stress, like cracks and craze fibrils, also supported voiding. The mechanism of the phase separation, loss of material and underlying chemical processes are very likely linked and the elucidation of these aspects as well as their exploitation will from the basis of a subsequent manuscript.

The integrity of the oxidized polypropylene-polyaminopropylsiloxane interface did not appear adversely affected by the ninhydrin reaction. Clearly, ammonium carboxylate bridges positioned along the oxidized surfaces had either contributed marginally to interfacial bonding, or more likely, these functional groups were simply not accessible to the ninhydrin reagent. In any case, scanning electron microscopy of ninhydrin-treated surfaces yielded identical images when compared to the aminopropylsilylated surfaces (figure 3, B versus C, respectively).

Conversion of aminopropylsilylated surfaces to the corresponding aldehyde. In this study, ninhydrin was used as well as glutaraldehyde to introduce surface-pendent aldehyde functional groups.

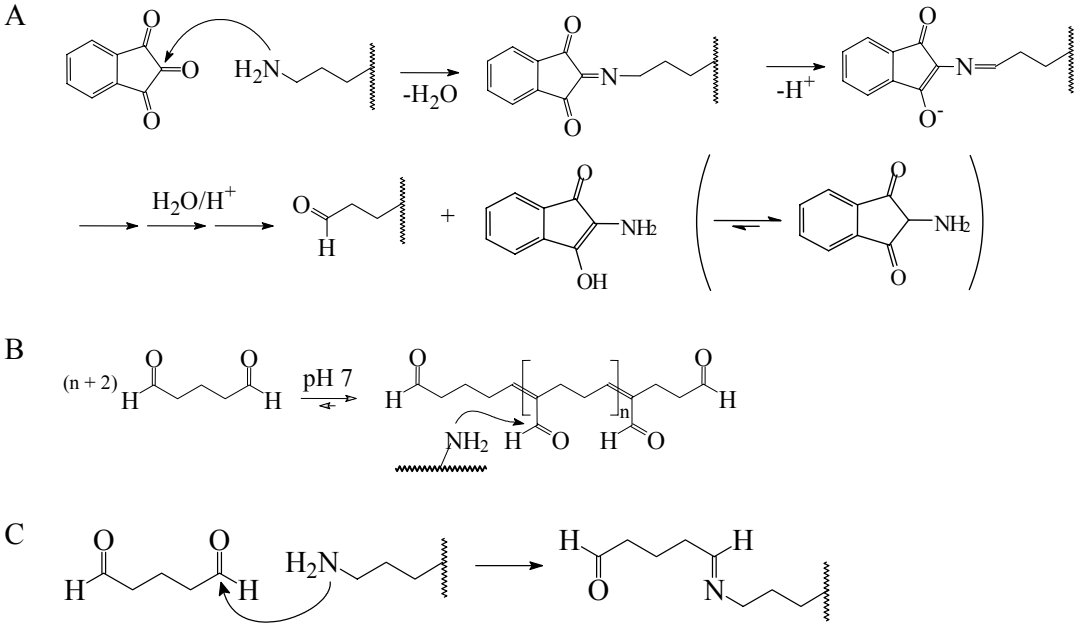

Figure 7. Reactions of immobilized primary amino groups with (A) ninhydrin, (B) polymeric glutaraldehyde, and (C) monomeric glutaraldehyde, to afford surfaces bearing reactive aldehyde species.

Figure 7 contrasts the chemistry of ninhydrin and glutaraldehyde-based routes to introducing aldehyde groups onto an amine-bearing surface. In the case of ninhydrin, the adduct, comprising one ninhydrin molecule and one surface amino group, rearranges and cleaves at the N-C bond, affording an aldehyde and liberating a bicyclic amine structure (figure 7A). Color is typically obtained when the liberated bicycle combines with a second ninhydrin molecule via imine bond, forming a chromophore (reaction not shown). Since color was obtained in this ninhydrin reaction, it followed to reason that solvent-accessible amino groups must have been converted into the corresponding aldehyde. Unlike the ninhydrin reaction, the surface reaction of glutaraldehyde at neutral pH values or above is dominated by the polymeric species as opposed to the monomeric state. At these pH values, glutaraldehyde self-polymerizes via many stepwise aldol condensations to form repeating units of α,β-unsaturated aldehydes (figure 7B). As depicted in the diagram, imine bonding predominates over conjugate addition of amino groups. The convenience of glutaraldehyde was put into question upon discovering the unusual mesotopology of oxidized polypropylene. In particular, concern was expressed over the possibility that the

quality of mesoscale structures would be cloaked by a comparatively thick overlay arising from the deposition of polymeric glutaraldehyde. Indeed, the common practice to illustrate the binding of monomeric glutaraldehyde to a surface is very often a gross oversimplification of the reality, which implicates a reactive polymer as the predominant species in most preparations. Figure 7C illustrates the commonly misrepresented chemistry of glutaraldehyde addition to aminated surfaces.

Shape-complementarity model of protein-surface adhesion. The current study examined an interesting system in the sense that a sponge-like topology was observed to facilitate protein loading and surface retention. A significant increase of surface area following oxidation (figure 2) correlated well with the higher fluorescence observed in the re-engineered surfaces (figure 4, row A; controls versus re-engineered surfaces). That being said, elucidating the mode of improved protein retention was another matter. Only the mesoscale sponge-like surfaces appeared to retain protein following several washes. The native plastic lost fluorescence almost immediately and aminated flat surfaces also lost protein relatively quickly. A plausible scenario (Figure 8) was conceived to reflect these findings and those related to works on mesoporous zeolites [2]. In this model, only surface discrepancies on the order of protein size are considered. For low protein concentrations, direct migration to the base of a groove (A) is portrayed as unlikely. Rather, protein is envisaged to adsorb along the tips (B), where surface access is kinetically easiest, and to migrate towards the base (C), where shape complementarity is best. Having reached the bottom (D), optimal protein-surface interactions are depicted to yield a tighter grip on the protein than is realized along a flat surface (E).

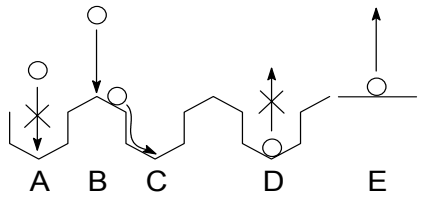

Figure 8. Protein retention along mesoscale curvatures

The nature of interactions, which are responsible for protein adsorption, have been debated for some time. Part of the confusion arises from the diversity of treatments, which attempt to rationalize binding phenomena. Quite often, different models, based upon

classical physics, have been used to relate surface-solute interactions and binding energies. Inherent to any model, important considerations are downplayed at times. With the onset of increased computing power, *in silico* work has served to reassess the binding problem more systematically, with particular attention placed on better balancing entropic and energy contributions. That being said, many simple treatments, whose origin is related to classically-defined hydrophobic, hydrophilic, charge, dipole and quadrupolar energy terms, to name a few, still show great utility in the matter of rationalizing protein binding.

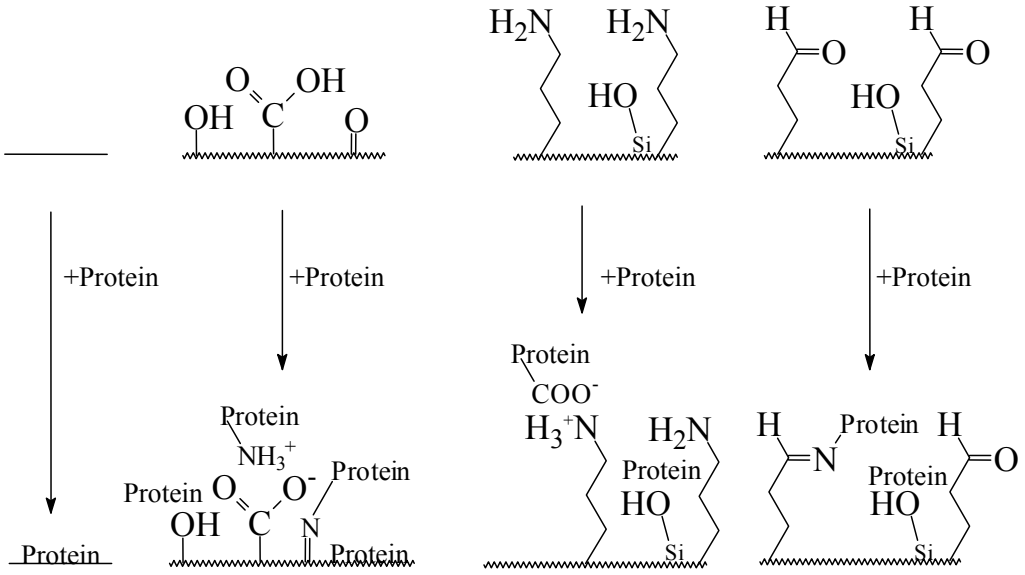

Figure 9. Multiple binding modes for protein retained along engineered surfaces. Surfaces are (A) native polypropylene; (B) oxidized polypropylene; (C) aminopropylsilylated oxidized polypropylene; and (D) aldehyde-transformed oxidized polypropylene.

While protein adsorption modes are subject to variation and protein-dependency, it is generally accepted that hydrophobic-hydrophobic interactions are the predominant factor responsible for protein binding along hydrophobic surfaces, whereas hydrophilic-hydrophilic interactions are the predominant factor responsible for binding along hydrophilic surfaces. In this classic sense, figure 9 illustrates the multiple binding modes for protein. Protein binding on native polypropylene (figure 9A) is dominated by hydrophobic interactions, particularly at pH values approaching the pI of the biomolecule. That being said, the bond is non-covalent. Binding to the oxidized surface is anticipated to reflect a composite effect of salt bridges, hydrogen bonding, covalent imine bonding, and possibly hydrophobic bonding in non-oxidized regions (figure 9B). With the formation of an imine bond, strong protein retention is expected. The aminopropylsilylated surface (figure 9C) presumably adheres protein by hydrogen-bonding to polar protein groups and

by forming salt bridges with protein carboxyl groups. Hydrogen bonds and salt linkages are reversible and should have a dependency on ionic strength. Like the ketone (figure 9B), the aldehyde group also binds proteins via imine formation (figure 9D). While simple imines are reversible in principle, the inertial bulk of a protein along a surface typically precludes desorption [?]. Glutaraldehyde-based imine linkages are truly irreversible, as the α,β-unsaturation confers enhanced stability to the imine bond [?]. Overall, the results indicate that all flat surfaces lose protein in time, barring covalent linkages, whereas shape-complementarity greatly aids protein retention in the absence of covalent bonding. In summary, it would appear that the most important factor to ensure protein retention in the absence of covalent bonding is a shape-conforming surface (figure 8). If this criterion is satisfied, the nature of individual interactions (figure 9) becomes relatively unimportant.

Conclusion

On the basis of this preliminary study, a reaction-induced phase separations permitted the development of an alternative mesoscale topology with greatly improved binding traits. While the example herein depicts an oxidation-induced phase-separation, many other reactive chemical approaches could potentially induce similar surface transformations and forge novel mesoscale topologies. Such strategies, if generalized, could provide alternatives to mesopattern problematic surfaces and to complement established methods based on lithography, self-organization and solvent casting.

Acknowledgements

This work was supported by Forschungszentrum Jülich, Germany, and Tübitak, Turkey, under project code ?????????????. A.T. thanks Mehmet Ali Gülgün of Sabancı University and İlhan Aksay of Princeton University for helpful suggestions.

Takahashi H., Li B., Sasaki T., Miyazaki C., Kajino T., Inagaki S.: Immobilized enzymes in ordered mesoporous silica materials and improvement of their stability and catalytic activity in an organic solvent. Microporous and Mesoporous Materials 44-45, 755-762, 2001.

[1] Karger-Kocsis, J. Polypropylene: An A-Z Reference, Kluwer Academic Publishers, NY, 1999.

[2] Arkles, B.: Tailoring surface with silanes. Chemtech 7: 766-778, 1977.

[3] Schertz, T.D., Reiter, R.C., Stevenson, C.D.: Zwitterion radicals and anion radicals from electron transfer and solvent condensation with the fingerprint developing agent ninhydrin. JOC 66: 7596-7603, 2001.

[4] Pavia L.D., Lampman G.M., Kriz G.S.: Introduction to Spectroscopy: A Guide for Students of Organic Chemistry, 3rd Edition, Thomas Learning Inc., USA, 2001.

[5] Hellan, K.: Introduction of Fracture Mechanics, McGraw-Hill Inc., NY, 1984.

[6] Jönsson, B., Lindman, B., Holmberg, K., Kronberg, B.: Interaction of Polymers with Surfaces: In Surfactants and Polymers in Aqueous Solution, John Wiley & Sons, NY, 1998.

[7] Yoon, J.-Y.; Kim, J.-H.; Kim, W.-S.: Interpretation of protein adsorption phenomena onto functional microspheres. Colloids and Surfaces B 12: 15-22, 1998. [8] March, J.: Advanced Organic Chemistry, 3rd edition, Wiley, NY, 1985.